

Multiwavelength study of a Solar Eruption from AR NOAA 11112 I. Flux Emergence, Sunspot Rotation and Triggering of a Solar Flare

Pankaj Kumar¹ · Sung-Hong Park¹ ·
K.-S. Cho^{2,3,1} · S.-C. Bong¹

© Springer

Abstract We analyse the multiwavelength observations of an M2.9/1N flare that occurred in the active region (AR) NOAA 11112 in the vicinity of a huge filament system on 16 October 2010. SDO/HMI magnetograms reveal the emergence of a bipole (within the existing AR) 50 hours prior to the flare event. During the emergence, both the positive and negative sunspots in the bipole show translational as well as rotational motion. The positive polarity sunspot shows the significant motion/rotation in the south-westward/clockwise direction and continuously pushing/sliding the surrounding opposite polarity field region. On the other hand, the negative polarity sunspot moves/rotates in the westward/anticlockwise direction. The positive polarity sunspot rotates $\approx 70^\circ$ within 30 hours, whereas negative polarity $\approx 20^\circ$ within 10 hours. SDO/AIA 94 Å EUV images show the emergence of a flux tube in the corona consistent with the emergence of the bipole in HMI. The footpoints of the flux tube were anchored in the emerged bipole. The initial brightening starts at one of the footpoint (western) of the emerged loop system, where the positive polarity sunspot pushes/slides towards a nearby negative polarity field region. A high speed plasmoid ejection (speed $\approx 1197 \text{ km s}^{-1}$) was observed during the flare impulsive phase, which suggests the magnetic reconnection of the emerged positive polarity sunspot with the surrounding opposite polarity field region. The entire AR shows the positive helicity injection before the flare event. Moreover, the newly emerging bipole reveal the signature of negative (left-handed) helicity. These observations provide the unique evidences of the emergence of twisted flux tube from below the photosphere to coronal heights triggering a flare mainly due to the interaction between the emerged positive polarity sunspot and a nearby negative polarity

¹ Korea Astronomy and Space Science Institute (KASI),
Daejeon, 305-348, Republic of Korea. email: pankaj@kasi.re.kr

² NASA Goddard Space Flight Center, Greenbelt, Maryland,
USA.

³ Department of Physics, The Catholic University of
America, Washington, D. C., USA.

sunspot by the shearing motion of the emerging positive sunspot towards the negative one. Our observations also strongly support the idea that the rotation is most likely attributed to the emergence of twisted magnetic fields, as proposed by recent models.

Keywords: Solar flare – coronal loops, magnetic field, flux rope, magnetic reconnection.

1. Introduction

Solar flares are one of the transient phenomena of magnetic energy release in the solar atmosphere. The magnetic energy stored in the twisted/sheared complex magnetic fields of active regions is converted into thermal and kinetic energies, as well as the acceleration of energetic particles via magnetic reconnection (Priest and Forbes, 2002; Chen, 2011). The emergence/activation of twisted flux tubes/ropes can lead to magnetic instabilities, interacting with the overlying fields and eventually result in the flare and associated eruption (Cho *et al.*, 2009; Kumar *et al.*, 2010c; Srivastava *et al.*, 2010; Foullon *et al.*, 2011; Kumar *et al.*, 2011). Using two dimensional magnetohydrodynamic (MHD) numerical simulation, Chen and Shibata (2000) proposed an emerging flux trigger mechanism for the onset of CMEs based on the flux rope model. Kink instability of the twisted magnetic flux ropes may also be responsible for the initiation of some solar eruptions (Török and Kliem, 2003; Török and Kliem, 2005; Kumar *et al.*, 2012a), and the interaction/reconnection between filaments/flux ropes may cause the eruption of the twisted magnetic fields (Kumar, Manoharan, and Uddin, 2010a; Török *et al.*, 2011). In addition, the coalescence of magnetic loops caused by footpoint shearing motion may also play an important role in flare triggering (Sakai *et al.*, 1986; Kumar *et al.*, 2010b). However, it is essential to investigate more exact mechanisms for the initiation of solar eruptive phenomena, because each flare and the associated dynamical processes may be unique in the energy build-up and release in associated active regions.

Rotating sunspots may be one of the most likely candidates to inject magnetic helicity into the solar atmosphere, which may cause the flare energy build-up (Stenflo, 1969; Barnes and Sturrock, 1972; Amari *et al.*, 1996; Tokman and Bellan, 2002; Török and Kliem, 2003; Régnier and Canfield, 2006; Zhang, Liu, and Zhang, 2008). Many pieces of observational evidence of sunspot rotation have been reported (e.g. several hundred degrees around their umbral centers over a few days) prior to the occurrence of strong flares (Brown *et al.*, 2003; Zhang, Li, and Song, 2007; Su *et al.*, 2008; Yan *et al.*, 2009; Min and Chae, 2009; Kumar, Manoharan, and Uddin, 2010a; Chandra *et al.*, 2011). The rapid rotation of the sunspots can cause the formation of sigmoidal loop that can erupt to produce flares and coronal mass ejections (Canfield, Hudson, and McKenzie, 1999; Pevtsov, 2002; Yan and Qu, 2007). The recent theories/models suggest that sunspot rotation can be caused by a pre-twisted magnetic flux tube emerging from below the photosphere (Longcope and Welsch, 2000; Gibson *et al.*, 2004; Magara, 2006; Fan, 2009). Tian and Alexander (2006) found sunspot

rotation as a primary driver of helicity production and injection into the corona and suggested that the observed active region dynamics, subsequent filament and sigmoid eruption are driven by a kink instability which occurred due to a large amount of the helicity injection. Tian, Alexander, and Nightingale (2008) suggested that the emergence of significantly twisted magnetic fields may not always result in the rotation of the associated sunspots, but they do play a very important role in the coronal helicity accumulation and free-energy build-up. Recently, Jiang *et al.* (2012) studied the sunspot evolution/rotation associated with the first X-class flare of the current solar cycle, which occurred in AR 11158 on 2011 February 15 and suggested that the shearing and rotational motions are the main contributors to the energy build-up and helicity injection leading to the flare, the cancellation and collision might act as a trigger. However, the exact cause and effect of rotating sunspots are not well understood up to now.

In this paper, we analyse the multiwavelength observations from *Solar Dynamic Observatory* (SDO: Pesnell, Thompson, and Chamberlin, 2012) to investigate the possible cause of energy build-up and triggering mechanism of a M-class flare that occurred in the AR NOAA 11112. In Section 2, we present multiwavelength observations of the M-class flare. In Section 3, we describe the evolution of magnetic field. In the last section, we discuss the results and draw the conclusions.

2. Multiwavelength Observations of M2.9/1N flare

The active region NOAA 11112 (β -type configuration) was located in southern hemisphere (S19W29) on 16 October 2010. The first flare (M2.9/1N) associated with a slow CME was observed in this active region (AR) on 16 October 2010. Later, this AR produced seven C-class flares during its passage through solar disk from 17-20 October 2010. Figure 1 displays the GOES soft X-ray flux (1-8 Å) and its derivative, *Ramaty High Energy Solar Spectroscopic Imager* (RHESSI: Lin *et al.*, 2002) hard X-ray fluxes in 12-25 keV (black) and 25-50 keV (red), and radio flux profiles in different frequency bands observed at the Sagamore Hill station. An M2.9-class flare started at 19:07 UT, peaked at 19:12 UT and ended at 19:15 UT. It was a short-duration flare. In $H\alpha$, it was classified as 1N class flare, which started at 19:10 UT, maximized at 19:13 UT and ended at 19:30 UT. The soft X-ray flux derivative matches the hard X-ray flux specially in 25-50 keV, which suggests that the same electrons are responsible for both thermal (SXR) and nonthermal (HXR) emissions, *i.e.*, the Neupert effect holds (Neupert, 1968; Veronig *et al.*, 2002). The radio flux profiles in different frequencies show a peak at 19:11 UT, which correlates well with the hard X-ray emission. The flux profile in 410 MHz shows two peaks prior to the main peak (19:11 UT). This may be related to the precursor of the flare and may correspond to the typical height of the reconnection. The decimetric bursts (100-4000 MHz) match with the hard X-ray emission, which are believed to be associated with the nonthermal electrons emitted by a coherent process (Benz *et al.*, 2005). Coherent radio emission at decimeter wavelengths originates in either a plasma density between 3×10^8 and 3×10^{10} cm³ or a magnetic field between 100 and 1000 G

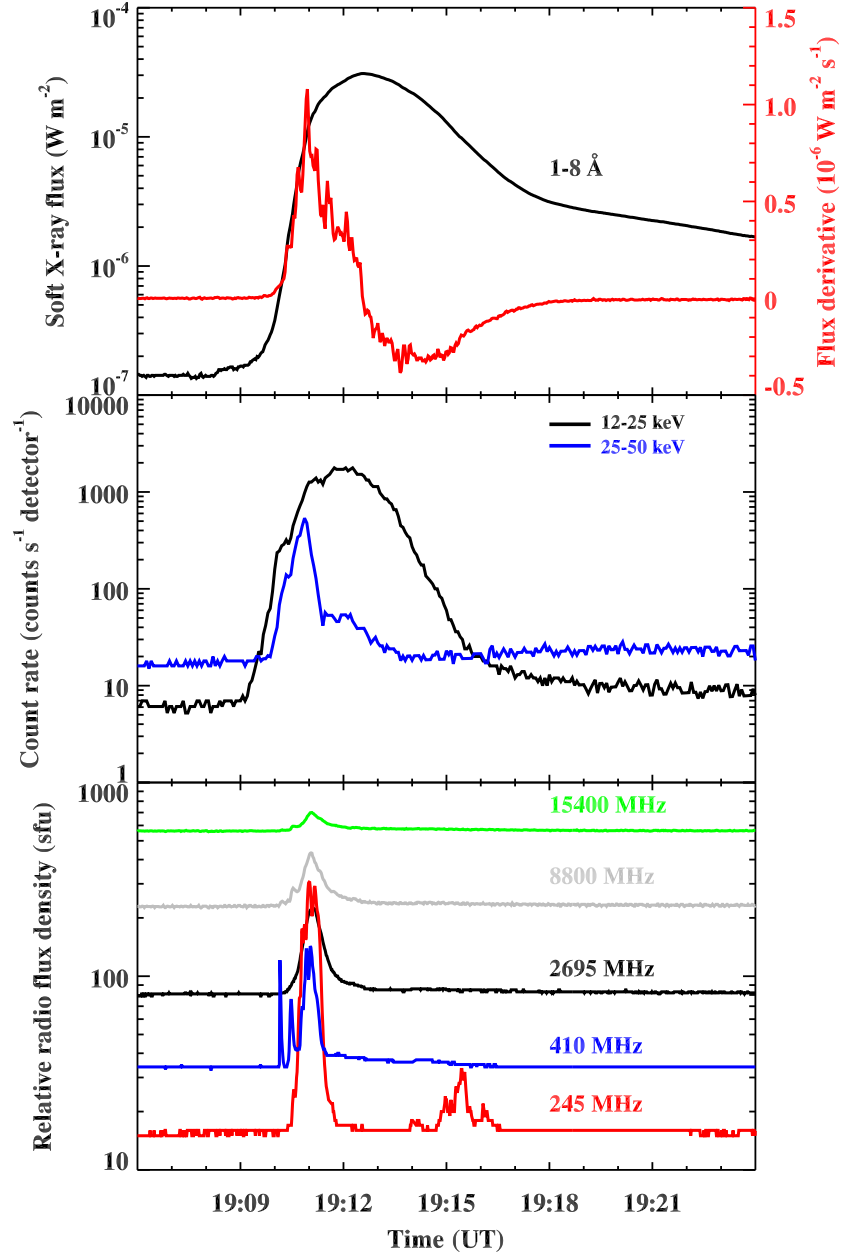


Figure 1. GOES soft X-ray flux profile and its derivative (red), RHESSI hard X-ray flux profiles in 12-25 keV (black) and 25-50 keV (blue) energy bands, and radio fluxes in 245, 410, 2695, 8800, 15000 MHz from Sagamore-Hill station on 16 October 2010.

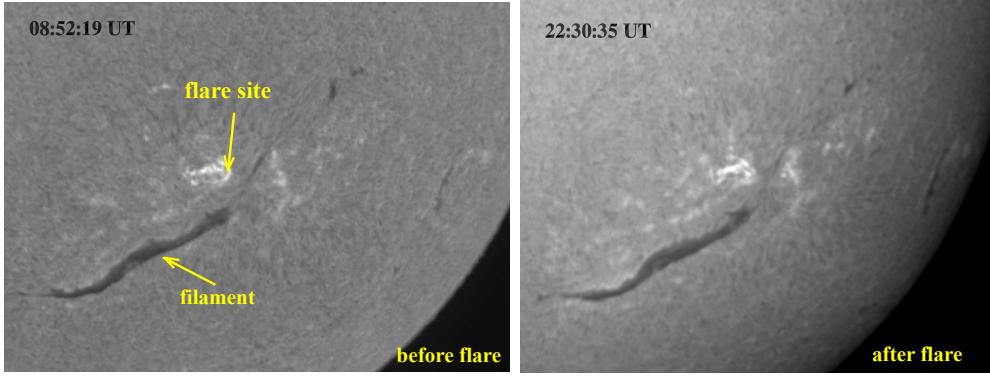


Figure 2. $H\alpha$ images observed from BBSO and SMART telescopes respectively before (left) and after (right) the flare. It may be noted that there is no filament eruption during the flare.

(assuming second harmonic emission is present), which are typically expected in flare acceleration regions (Dabrowski and Benz, 2009).

Figure 2 displays the $H\alpha$ images of the active region before (08:52:19 UT) and after (22:30:35 UT) the flare observed respectively at Big Bear Solar Observatory (BBSO) and with the *Solar Magnetic Activity Research Telescope* (SMART) (Ueno *et al.*, 2004). The active region was associated with a huge filament lying along southeast direction. The flare occurred not far from the filament, which did not erupt during the flare event.

SDO/*Atmospheric Imaging Assembly* (AIA: Lemen *et al.*, 2012) observes multiwavelength images at $0.6''$ per pixel resolution with 12 s cadence. The field of view is $1.3R_{\odot}$, so it covers the full solar disk. We use the AIA 211 Å (Fe XIV, $T \approx 2$ MK), 304 Å (He II, $T \approx 0.05$ MK), 1700 Å ($T=5000$ K) and 94 Å (Fe XVIII, $T \approx 6.3$ MK) images, which cover the height from the photosphere to the corona. Figure 3 displays SDO/AIA 94 Å EUV images, revealing the coronal configuration of the active region and associated flare brightening. These images are favorable to observe the evolution of high temperature plasma in the flaring region. The top-left panel has been overlaid by *Helioseismic and Magnetic Imager* (HMI: Schou *et al.*, 2012) magnetogram contours of positive (white) as well as negative polarities (black). This shows the connectivity of the footpoints of the corresponding loop-systems before the flare. Careful inspection of these images reveals the existence of two major loop systems in the active region. The top-right image shows one longer loop system in the westward direction (indicated by “W-loop”), whereas a smaller loop system was protruding in the eastward direction (indicated by “E-loop”). The footpoint polarities of these loops are indicated by ‘+’ and ‘-’ symbols. The flare brightening started at the western footpoint of the E-loop system in between the opposite-polarity regions (indicated by arrow).

A plasmoid ejection was also observed during the flare impulsive phase (19:10:26 UT to 19:10:50 UT). The panel at 19:10:26 UT shows the plasmoid ejection indicated by arrow. The moving plasmoid structure is revealed in the panels at 19:10:38 UT and 19:10:50 UT (marked by arrows). We measured the distance of the plasmoid’s leading edge from the flare center and calculated the speed from

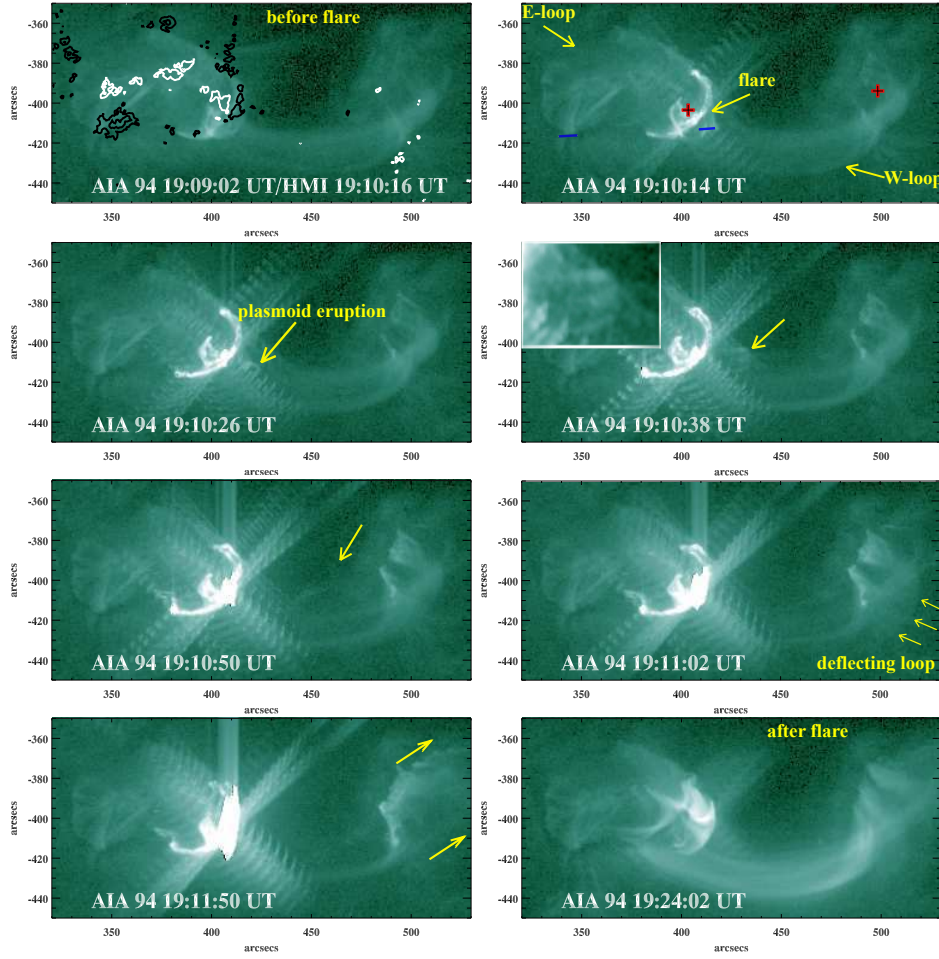


Figure 3. Selected SDO/AIA 94 Å EUV images showing the initiation of M2.9 flare associated with plasmoid eruption and deflection of loop system on 16 October 2010. The top-left image has been overlaid by HMI magnetogram contours of positive (white) and negative (black) polarities. The contour levels are ± 500 , ± 1000 , ± 2000 and ± 3000 gauss (G). The enlarged view of the plasmoid is shown in the top-left corner of a panel at 19:10:38 UT.

the linear fit to the projected height-time measurements, which was $\approx 1197 \text{ km s}^{-1}$. Moreover, we observe a strong deflection at the right footpoint of the W-loop system just after the plasmoid's disappearance during the flare peak time at 19:11:02 UT (please see AIA 94 Å movie). The deflection at the footpoint of the loop system is likely caused by the propagation large scale coronal wave away from the flare site, which is studied in detail in Kumar *et al.* (2012b)(hereafter Paper II). After the flare (19:24:02 UT), we can see the two loop systems as observed prior to the flare event. It should be noted that these two loop-systems are filled with hot plasma as evident in 94 Å images. Therefore, AIA images show the coronal environment at the flare site, associated flare brightening, plasmoid ejection as well as rearrangement of the loop systems. Most of the

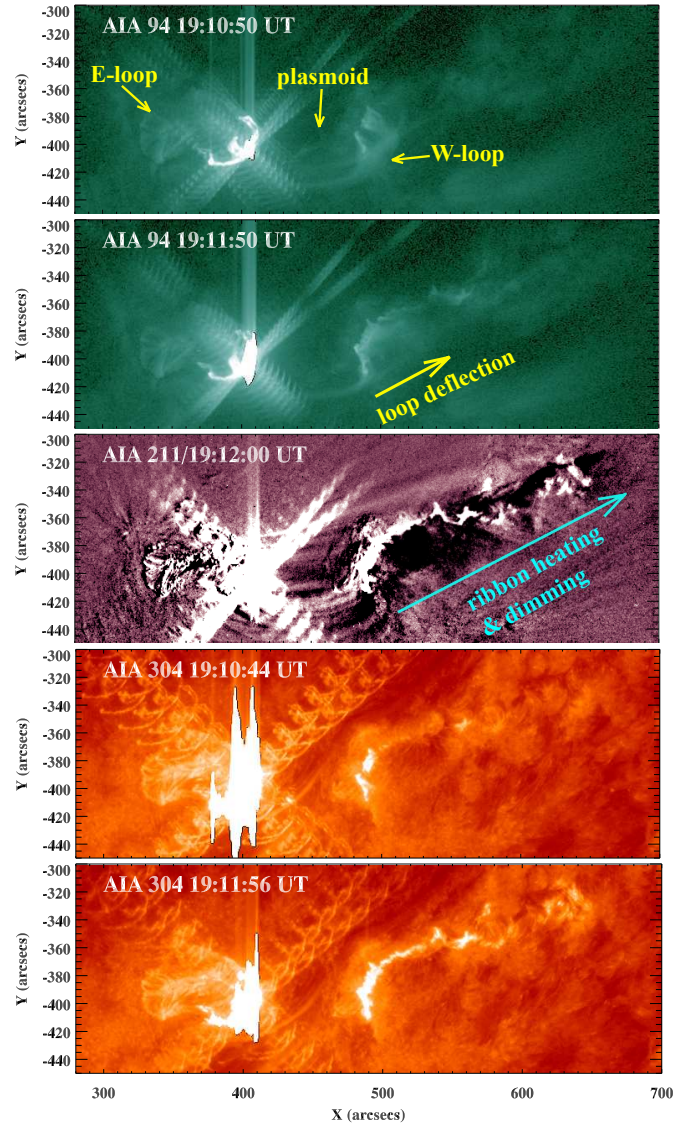
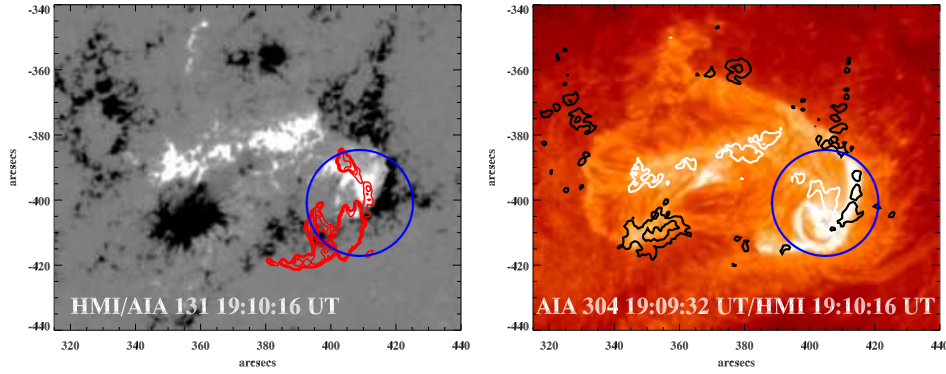


Figure 4. Selected SDO/AIA 94, 211 (base difference) and 304 Å EUV images showing the deflection of the W-loop by a westward propagating disturbance and associated extended ribbon brightening.

nonthermal emission in hard X-ray (25-50 keV) as well as in radio flux profile peaked at 19:11 UT (Figure 1), during the acceleration phase of the plasmoid. This scenario conforms with the standard eruptive flare model (i.e. CSHKP), where the nonthermal emission matches well with the timing of plasmoid acceleration (Ohyama and Shibata, 1998; Yokoyama and Shibata, 2001; Maričić *et al.*, 2007; Temmer *et al.*, 2008; Temmer *et al.*, 2010).



The contour levels are ± 500 , ± 1000 G. White/Black contours indicate positive/negative polarities.

Figure 5. Left: SDO/HMI magnetogram overlaid by AIA 131 Å image intensity contours. The contour levels are 30%, 50%, 70%, 90% of the peak intensity. Right: HMI magnetogram contours overlaid on AIA 304 Å image during the initial phase of the flare.

In order to illustrate the deflection of the W-loop and associated coronal and chromospheric responses of the flare, we have shown some of the selected AIA images in 94, 211 and 304 Å in Figure 4. AIA 94 Å images show the westward deflection of the W-loop (indicated by an arrow), just after the plasmoid ejection (top two panels). We can see the extended ($\approx 200''$) ribbon brightening in AIA 211 Å base difference image at 19:12 UT. The flare ribbon is also observed in AIA 304 Å (i.e. chromosphere and transition region) images. In AIA 94 and 211 Å movies, we see the propagating disturbance in the western direction starting from the flare center. The coronal dimming along the direction of propagating brightening probably indicates the depletion of density. The deflection of the coronal W-loop and ribbon brightening may be associated with a coronal wave propagating from the flare site. A detailed study of the coronal wave is presented in Paper II.

Figure 5 displays HMI magnetogram and AIA 304 Å image. The left image shows the HMI magnetogram overlaid by AIA 131 Å flare intensity contours. The contour levels are 30%, 50%, 70%, and 90% of the peak intensity. It is noted that the flare brightening in corona was located above a pair of small opposite polarity field regions (shown within the circle). The right image displays HMI magnetogram contours over AIA 304 Å image during the flare initiation. AIA 304 Å image corresponds to upper chromosphere as well as the transition region of the solar atmosphere. The initial brightening started in between the opposite polarity bipolar region as indicated within blue circle.

3. Magnetic Field Evolution

We used the HMI magnetograms to follow the evolution of magnetic fields before and after the flare. HMI is designed to study oscillations and the magnetic field at the photosphere (Scherrer *et al.*, 2012). It observes the full solar disk ($4K \times 4K$)

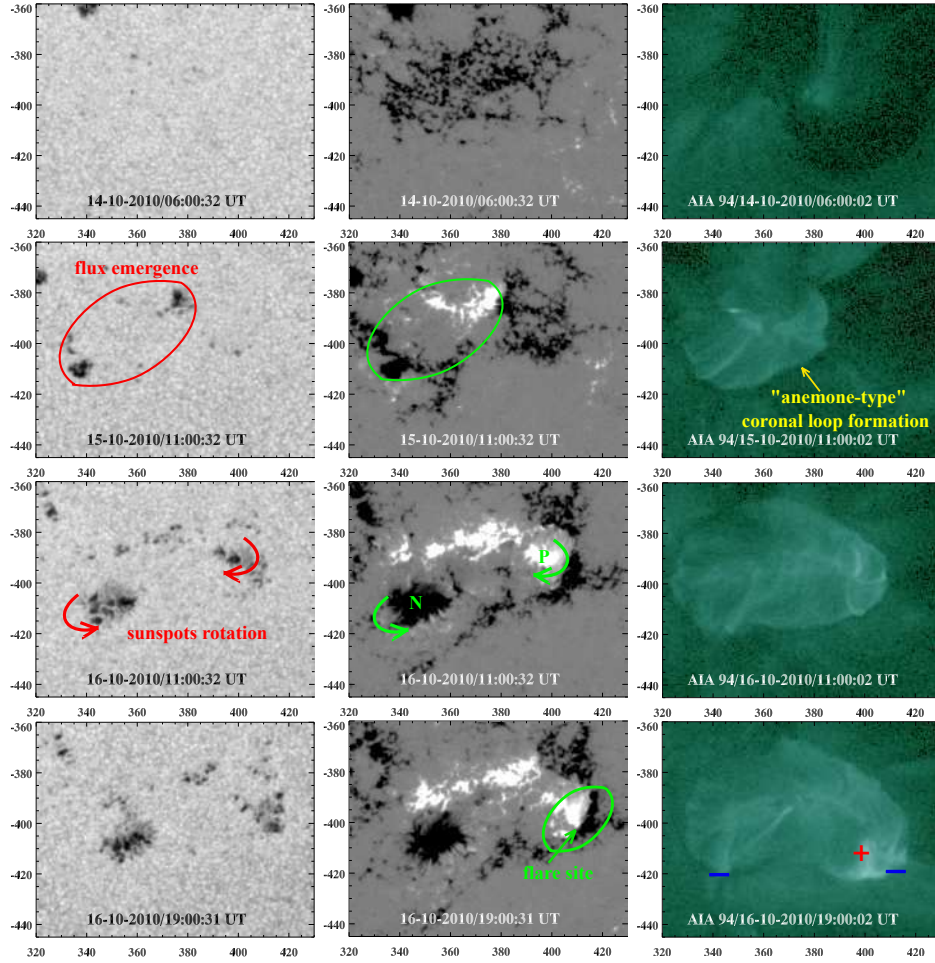


Figure 6. HMI continuum, magnetograms and AIA 94 Å EUV images before the flare occurrence. X and Y axis are in arcsecs.

at 6173 Å with a resolution of $1''$ ($0.5'' \text{ pixel}^{-1}$). The typical cadence for magnetograms is 45 s. The magnetogram image shows the photospheric magnetic field, with black and white indicating negative and positive polarities, respectively. We have used the HMI continuum images to follow the morphological evolution of the sunspots. In order to see the morphological evolution of the sunspots at the photosphere and associated responses at the coronal heights, we compared co-temporal HMI continuum, magnetograms and AIA 94 Å EUV images. Figure 6 displays the HMI continuum, magnetograms as well as AIA images from 14 October to 16 October 2010. The top row panels display pre-flux-emergence images. The emergence of opposite polarity sunspots started at 18:00 UT on 14 October 2010 and the sunspot pair grew continuously (please see HMI movie). The panels in the second row from the top show the emergence of a bipole indicated inside the ellipse in HMI images. It is interesting to note that we

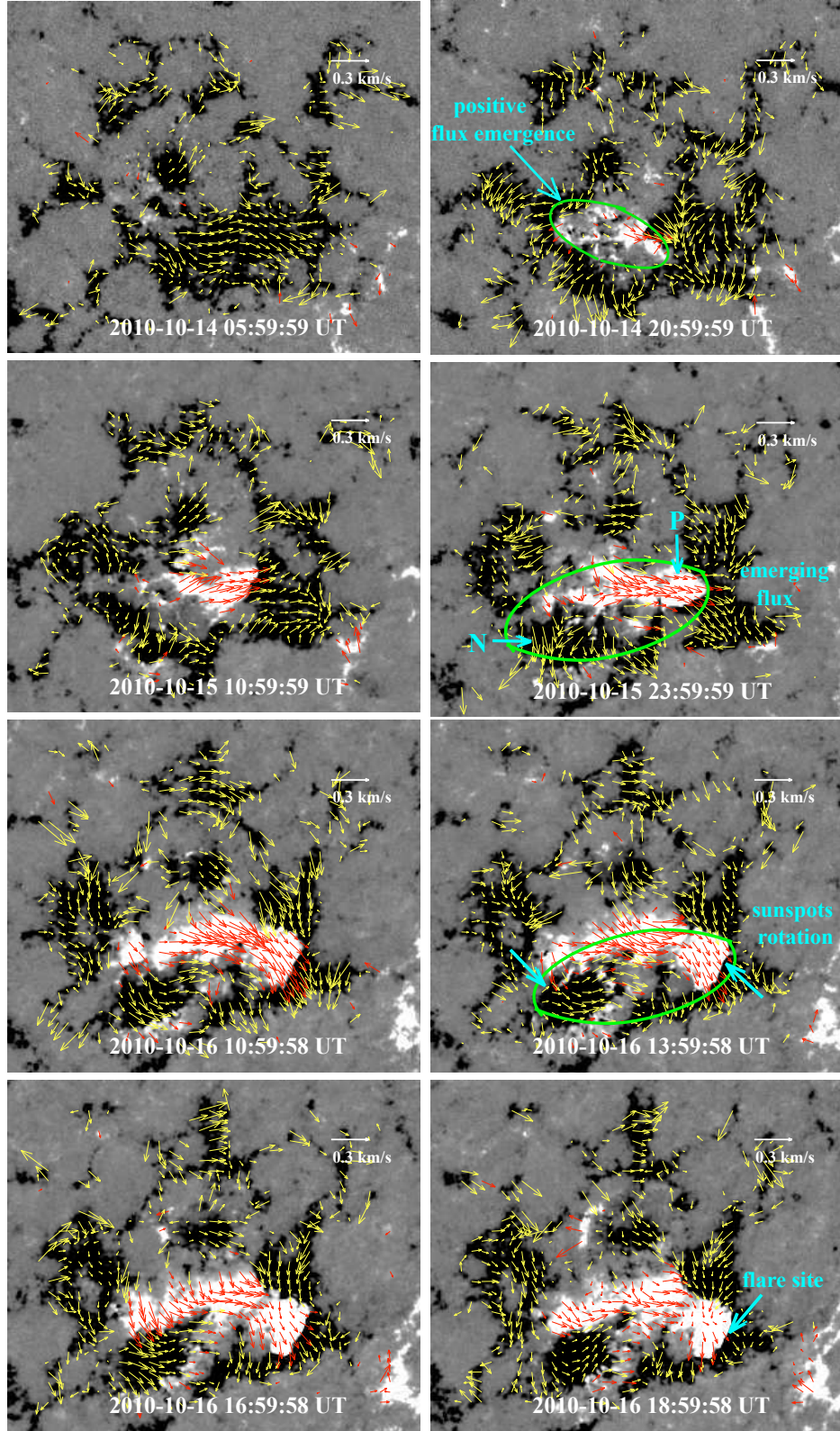


Figure 7. Photospheric flow maps of the flare site obtained by DAVE technique using HMI magnetograms. The size of each image is $164'' \times 140''$. The magnetic field is scaled in the above images -200 G to +200 G.

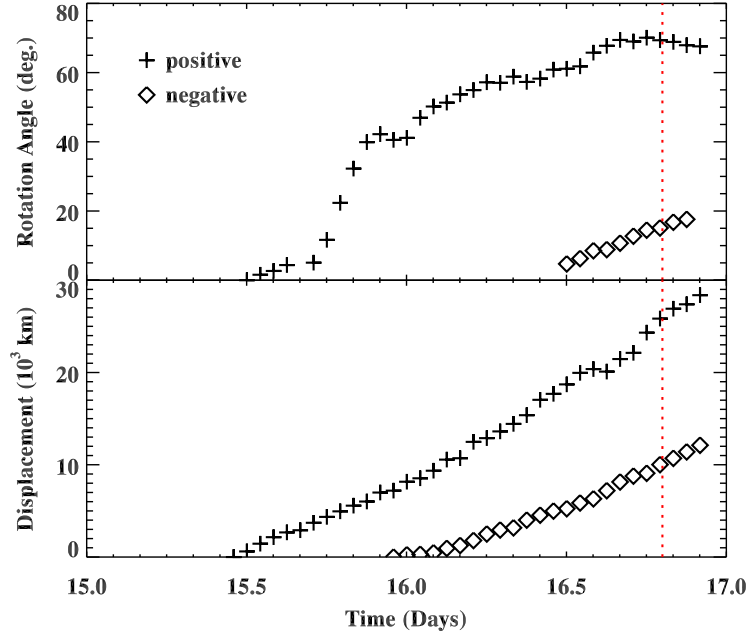


Figure 8. Upper panel: Temporal evolution of the accumulated rotation angle of both the positive and negative polarity sunspots on 15 and 16 October 2010. The absolute values of the rotation angle have been plotted for the negative polarity sunspot. Lower panel: Accumulated displacement of the center position of both sunspots. The vertical dotted line indicates the flare peak time on 16 October 2010.

see the emerging of “anemone-type” coronal loop system in AIA 94 Å image (indicated by arrow) at the same time. After the emergence, positive polarity sunspot (‘P’) shows rotation in the clockwise direction. On the other hand, the negative polarity sunspot (‘N’) rotates in anticlockwise direction (detected in HMI images). The comparison between HMI and AIA images reveals that the footpoints of the emerged loop system are anchored in the emerged opposite polarity sunspots and moves as the sunspots move/rotate. This is a good example of emergence of a flux tube from below the photosphere to coronal heights. Further, the shape of the emerged loop seems to have a twisted field configuration. The structure/orientation of the field lines in the flux tube can be viewed. The helicity sign can be characterised by the presence of elongated polarities, called “magnetic tongues” of the emerging flux-rope (refer to Figures 1 and 3 in Luoni *et al.* (2011) for the detail way to determine the helicity sign). Therefore, here the line of sight magnetic field distribution in the emerging bipole indicates negative (left-handed) helicity.

3.1. Photospheric Flow Maps

To deduce the photospheric flows, we selected hourly magnetograms from 14-16 October 2010 (before the flare event). We have used Differential Affine Velocity Estimator (DAVE) technique (Schuck, 2005; Schuck, 2006; Chae and Sakurai,

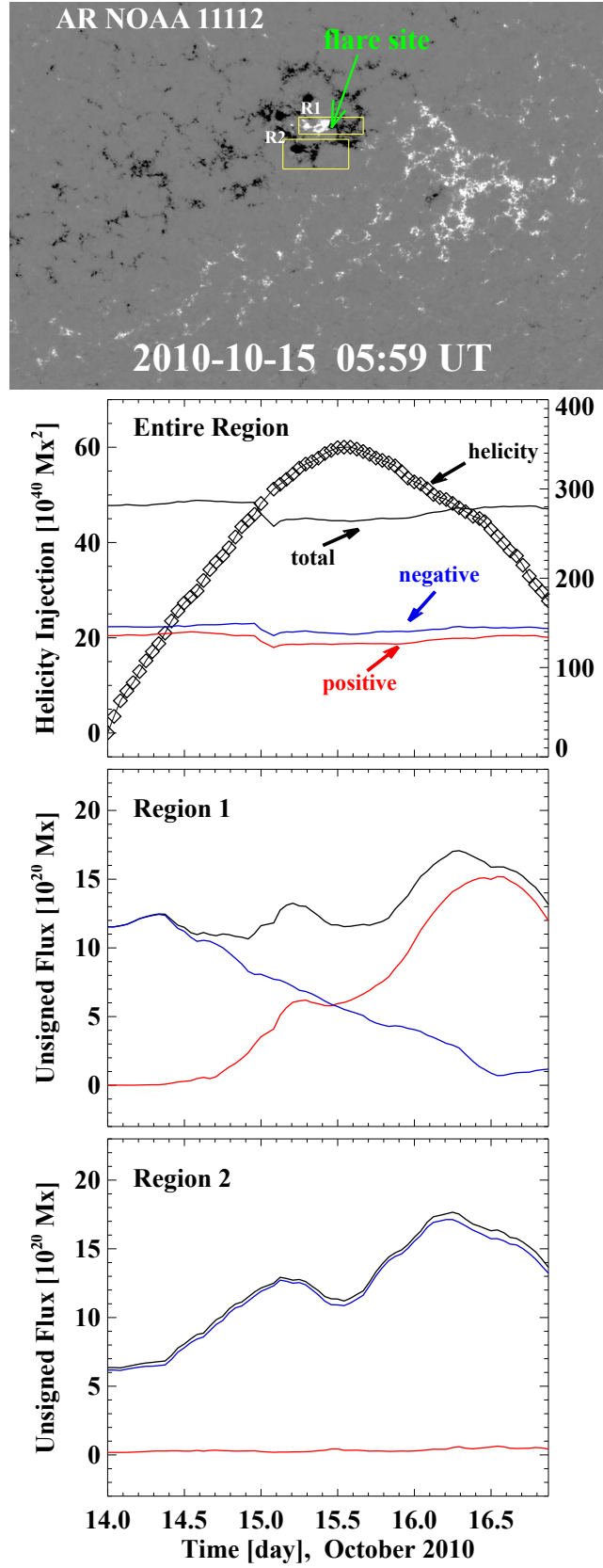


Figure 9. Top panel: HMI magnetogram of the NOAA AR 11112 on 15 October 2010. Region 1 and region 2 are shown by boxes indicated by 'R1' and 'R2' respectively. The image size is $644'' \times 412''$. Bottom panel: Evolution of magnetic helicity (diamond), positive (red), negative (blue) and total (black) unsigned magnetic flux profiles beginning from 14 October 2010.

2008) for the estimation of photospheric flows. After many trials, we choose the width of Gaussian window $10''$. Figure 7 displays selected flow maps obtained with the DAVE technique. It is interesting to see the emergence of positive flux on 14 October 2010 and later the emergence of a bipole (indicated by ‘P’ and ‘N’) is more clear on 15 October 2010 (indicated by arrows). The positive flux emerges and moves towards the western side. The direction of flow arrows strongly suggests that the positive polarity sunspot rotates in the clockwise direction and pushes/slides towards the neighbouring opposite (negative) polarity field region in southwest direction. This helps in increasing the shear and build-up of magnetic energy in between opposite polarity field regions, which is being released later in the flare. Therefore, the interaction of the two opposite polarity regions (indicated as flare site) was the most likely cause for triggering the flare. On the other hand, the flow arrows for the emerging negative polarity sunspot (‘N’) shows anticlockwise rotation specially on 16 October 2010.

3.2. Measurement of Sunspot Rotation

The emerged opposite polarity sunspots showed translational as well as rotational motion before the flare occurrence. The emerged positive polarity has an elliptical shape. Its orientation can be described by an angle between its major axis and the equator in anticlockwise direction. The rotation rate is defined as the orientation change in two successive images of the sunspot. In order to measure the rotation angle of both sunspots, we use `fit_ellipse` routine available in IDL library. The sunspot structure is defined as a region having magnetic field $\geq 10\%$ of the peak field strength. This procedure provides the center position as well as the orientation of the best-fitted ellipse on the sunspot region. Figure 8 displays the temporal evolution of the accumulated rotation angle (upper panel) as well as accumulated displacement of the center position (lower panel) of positive (+) and negative (diamond) polarity sunspot. The emerged positive polarity sunspot started to rotate in the clockwise direction on 15 October 2010 at 12:00 UT and showed significant rotation ($\approx 40^\circ$) till 23:00 UT. Later, it continued to rotate gradually on 16 October 2010 and the rotation angle becomes nearly constant 2-3 hours before the flare occurrence. Therefore the total rotation angle for the positive polarity sunspot was $\approx 70^\circ$ within 30 hours. On the other hand, the emerged negative polarity sunspot does not show any detectable significant rotation on 15 October, while it shows slow rotation in the anticlockwise direction on 16 October 2010 (see Figure 8 upper panel). The total rotation angle for the negative polarity sunspot was $\approx 20^\circ$ within 10 hours. Therefore, the rotation rates for the positive and negative polarity sunspots are ≈ 2.3 and 2° h^{-1} respectively, which are comparable. Apart from the rotational motion, both sunspots also show a translational motion (divergence) after the emergence (refer to lower panel of Figure 8). The positive polarity sunspot shows a significant displacement after the emergence and moves ≈ 26 Mm within 30 hours in the southwest direction. On the other hand, negative polarity sunspot moved westward ≈ 12 Mm within 22 hours. The significant and continuing displacement as well as the rotation of positive polarity sunspot helped in the build-up of magnetic energy to trigger the flare.

3.3. Estimation of Helicity Injection

Magnetic helicity is a useful measure for global complexity and non-potentiality of a magnetic field system (Berger and Field, 1984; Pevtsov, 2008; Démoulin and Pariat, 2009) and it has been studied to understand an energy build-up process, pre-flare conditions, and triggering mechanisms of flares (Kusano *et al.*, 2003; LaBonte, Georgoulis, and Rust, 2007; Park *et al.*, 2008; Park, Chae, and Wang, 2010). We therefore determined magnetic helicity injection through the photospheric surface of the active region (AR) NOAA 11112 to quantify the temporal evolution of complexity built up by motions of magnetic fragments in sunspot areas of the flare-producing active region.

To measure the magnetic helicity injection, we first calculated helicity flux density $G_\theta(\mathbf{x}, t)$ (i.e., helicity injection per unit area per unit time) at a position \mathbf{x} on the photospheric surface of AR 11112 and a specific time t using the helicity flux density formula proposed by Pariat, Démoulin, and Berger (2005) and the numerical calculation method developed by Chae (2007):

$$G_\theta(\mathbf{x}, t) = -\frac{B_n}{2\pi} \int_{S'} \left(\frac{\mathbf{x} - \mathbf{x}'}{|\mathbf{x} - \mathbf{x}'|^2} \times [\mathbf{u} - \mathbf{u}'] \right)_n B'_n dS', \quad (1)$$

where the subscript n denotes the vertical component to the photospheric surface S' of the active region. B_n is the magnetic field component perpendicular to S' and it is derived from the line-of-sight component B_l by assuming that the transverse component of magnetic fields is negligible compared to B_l (i.e., $B_n = B_l / \cos \psi$ where ψ is the heliocentric angle). \mathbf{u} is the velocity of the apparent horizontal motion of field lines determined by applying the differential affine velocity estimator (DAVE) method (Schuck, 2006). In this study, $G_\theta(\mathbf{x}, t)$ was determined using SDO/HMI line-of-sight magnetogram data in the time span of 14 October 2010, 00:00 UT through 16 October 2010, 21:00 UT with a 1-hour cadence. Then the amount of helicity injection $H(t)$ through a local region S_R in the active region is determined by integrating $G_\theta(\mathbf{x}, t)$ with respect to the area of S_R and time:

$$H(t) = \int_{t_0}^t \int_{S_R} G_\theta(\mathbf{x}, t) dS_R dt, \quad (2)$$

where t_0 is the start time of the magnetogram data set under investigation.

We have estimated the helicity injection, positive flux, unsigned negative and total unsigned magnetic flux in the entire active region as well as magnetic flux profiles in the regions of the localized emerged polarities. Top panel of Figure 9 displays the HMI magnetogram of the AR, where R1 and R2 indicate the emerging flux regions for positive and negative polarities respectively. The flare site is indicated by an arrow. The temporal variations of helicity injection (diamond), positive (red), unsigned negative (blue) and total (black) unsigned magnetic flux have been displayed in the bottom panel of Figure 9. The entire AR shows the injection of relatively more positive helicity starting from 14 October 2010, peaking ($\approx 60 \times 10^{40} \text{ Mx}^2$) at 12:00 UT on 15 October 2010 and later it presents a relatively more negative helicity injection. Region 1 (R1) shows the emergence of

positive flux on 14 October ($\approx 12:00$ UT), first peak on 15 October and enhances significantly ($\approx 15 \times 10^{20}$ Mx) on 16 October before the flare triggering. Please note that the decrease in the negative flux in R1 is due to the pushing/sliding motion of the positive polarity, which make the negative polarity to move out from the box region R1. Region 2 (R2, bottom panel) displays the increase in the negative flux (maximum value $\approx 17 \times 10^{20}$ Mx) same as the increase of the positive flux in R1. The entire active region has a magnetic inversion line, which is oriented nearly at 45° to the solar equator. As it was shown by Démoulin *et al.* (2002), the helicity injection by differential rotation changes sign when the AR's inversion line becomes more tilted than 45° . On the south hemisphere, the initial positive helicity injection in the entire region later becomes negative, i.e. the total coronal helicity starts to be depleted by differential rotation. We believe that this may be the case here, besides the negative helicity injection by the new bipole. The entire picture of magnetic helicity in the active region might be as follows: (1) at first, until the middle of 15 October, positive helicity was injected through the photospheric surface of a much larger and dispersed bipole (*i.e.*, pre-existing bipole) which covers the entire region of NOAA 11112. But negative helicity starts to be injected through the pre-existing bipolar region by the differential rotation from the middle of 15 October, and (2) the newly emerging bipole has pre-twisted magnetic fields with negative sign, which can be estimated from the study of Luoni *et al.* (2011) and their footpoints show the rotation in opposite directions due to bodily rotation of the bipolar flux tube (rotating as a whole). The important thing to note is that the emerging flux profiles for the positive and negative polarities are quite similar in region R1 and R2, which strongly suggests the emergence of a flux tube from below the photosphere. The coronal signature of emerging flux in the form of “anemone-shaped” loop system, is confirmed in AIA 94 Å images (Figure 6).

4. Discussion and Conclusions

We have analysed the multiwavelength observations of the M2.9/1N flare occurred on 16 October 2010 from AR NOAA 11112. SDO Observations reveal the emergence of flux tube within the existing AR from below the photosphere to the corona. The footpoints of the emerged bipole show the rotation in opposite directions. The positive polarity sunspot shows a significant rotation in the clockwise direction during ≈ 30 h before the flare, whereas negative polarity sunspot shows a relatively smaller rotation in the anticlockwise direction during ≈ 10 h before the flare triggering. Moving/rotating positive polarity sunspot continuously pushes the negative polarity field region towards southwest direction. The shear motion of this sunspot helped in the build-up of magnetic energy and the flare was triggered when the magnetic configuration became unstable. Moreover, the photospheric flow map also confirms the sliding motion of the positive sunspot in the southwest direction. Kurokawa (1987) found two type of processes for the development of magnetic shear configurations between sunspots: (a) collision of two sunspots of opposite magnetic polarities, and (b) successive emergence of twisted magnetic flux ropes. He suggested that the second process might

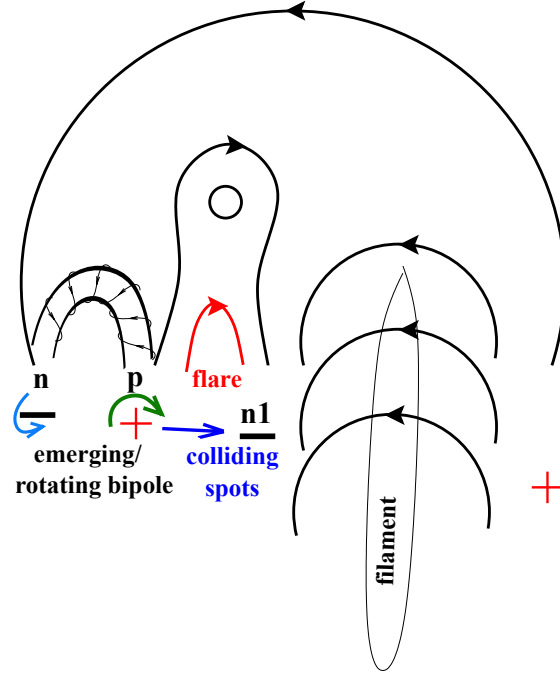


Figure 10. Schematic cartoon showing the emerged flux tube, plasmoid ejection and associated magnetic reconnection at the flare site.

be essential for the production of big flares. The present event indicates both processes, *i.e.*, emergence as well as the sunspot collision, which are responsible for the development of magnetic shear to trigger the M-class flare.

Figure 10 displays the schematic cartoon to show the magnetic field environment of the flare site. The energy build-up and release process can be explained in the following way: (i) ‘n’ and ‘p’ displays the emerging and rotating bipole in opposite directions, (ii) field lines in the emerged loop shows left-handed twist, whose footpoints are anchored in the rotating spots ‘n’ and ‘p’, (iii) clockwise rotating/sliding sunspot ‘p’ collides with opposite polarity spot ‘n1’, (iv) magnetic reconnection takes place in between colliding spots (‘p’ and ‘n1’) and a plasmoid was ejected followed by an M-class flare. The first reconnection most likely started in the lower solar atmosphere, which was confirmed by the high frequency decimetric radio bursts profiles. The location of the RHESSI hard X-ray sources and initial ribbon brightening during the flare impulsive phase suggest the reconnection of field lines between two opposite polarity colliding spots. The plasmoid ejection during the flare impulsive phase is an indirect evidence of magnetic reconnection (Shibata *et al.*, 1995).

The emerging bipoles generally show the rotation in the same direction, which generates a sheared polarity inversion line. This process creates the sigmoid structure in the corona that shows ‘S’ or ‘inverse-S’ shape in soft X-rays (Pevtsov, Canfield, and Metcalf, 1995; Rust and Kumar, 1996; Canfield, Hudson, and McKenzie, 1999). These sigmoid structures are generally considered to produce

flares/CMEs. The present event shows the emergence of a flux tube associated with footpoints/sunspots rotation in opposite directions. This may explain why sigmoid was not formed and why the flux tube did not erupt. Although the footpoints rotate in opposite directions, the total rotation-angles are different, which implies that the rope was twisted by this process. A bodily rotation of a flux tube (rotating as a whole) injects no net helicity in the system, though locally rotation is seen (refer to Pariat, Démoulin, and Nindos, 2007). However, the observation that the two opposite polarity spots rotate in opposite directions indicates that there is an additional global positive, right-handed rotation of the emerging flux rope (i.e. the flux rope is rotating as a whole). We believe that here we have a superposition of a flux rope emerging with negative helicity (as shown by the magnetic tongue/tails structure, and a smaller rotation of the flux rope as a whole). Yan, Qu, and Kong (2008) proposed that the two sunspots with the same rotating direction have higher flare productivity than those with opposite rotating directions, and this scenario makes it easier to store magnetic energy and increase the helicity of the flux tube. Indeed, the present AR was not large flare/CME productive and the first flare (M2.9) was observed on 16 October 2010 associated with a slow CME (speed ≈ 350 km s $^{-1}$).

Our observations show the flux emergence and rotation of sunspots simultaneously. This reveals the important aspects about the origin and effect of sunspot rotation, which is consistent with the idea suggested by many authors, that the rotation might result from the emergence magnetic fields pre-twisted below the photosphere (Brown *et al.*, 2003; Tian and Alexander, 2006; Min and Chae, 2009). Chae *et al.* (2003) proposed that a variety of shearing motions and rotational motions observed in ARs may be driven by the torque caused by the expansion of the coronal part of the twisted flux tube. Min and Chae (2009) suggested that if an initially twisted flux tube emerges, the coronal segment of the tube is likely to expand due to the pressure difference between the interior and the corona. In this case, a magnetic-torque imbalance (Jockers, 1978) occurs between the expanded part (corona) and the unexpanded part (interior). So, the Lorentz force and the related torque on the photospheric boundary drive the sunspot rotation. We also notice the expansion in the emerging flux tube in the corona, which is in agreement with the above explanation.

In conclusion, we presented the multiwavelength observations of an M-class flare to show that its energy build-up was done by shearing and rotation of the positive polarity sunspot. The flare was triggered by the collision of positive polarity sunspot with the surrounding opposite polarity field region. Using the high spatial and temporal data from space and ground based instruments, further studies should be performed in order to shed more light on the flare triggering processes.

Acknowledgements We express our gratitude to the referee for providing the constructive comments/suggestions, which improved the manuscript considerably. SDO is a mission for NASA's Living With a Star (LWS) Program. We are thankful for the radio data obtained from RSTN network and GBRSSBS. Global High Resolution H α Network is operated by the Space Weather Research Lab, New Jersey Institute of Technology. PK thanks to Prof. P.F. Chen and Dr. A. K. Srivastava for fruitful discussions. This work has been supported by the "Development of Korea Space Weather Center" project of KASI, and the KASI basic research fund.

References

- Amari, T., Luciani, J.F., Aly, J.J., Tagger, M.: 1996, Very fast opening of a three-dimensional twisted magnetic flux tube. *Astrophys. J. Lett.* **466**, 39–42. doi:10.1086/310158.
- Barnes, C.W., Sturrock, P.A.: 1972, Force-free magnetic-field structures and their role in solar activity. *Astrophys. J.* **174**, 659–670. doi:10.1086/151527.
- Bárta, M., Karlický, M., Žemlička, R.: 2008, Plasmoid dynamics in flare reconnection and the frequency drift of the drifting pulsating structure. *Solar Phys.* **253**, 173–189. doi:10.1007/s11207-008-9217-5.
- Benz, A.O., Grigis, P.C., Csillaghy, A., Saint-Hilaire, P.: 2005, Survey on solar X-ray flares and associated coherent radio emissions. *Solar Phys.* **226**, 121–142. doi:10.1007/s11207-005-5254-5.
- Berger, M.A., Field, G.B.: 1984, The topological properties of magnetic helicity. *Journal of Fluid Mechanics* **147**, 133–148. doi:10.1017/S0022112084002019.
- Bradley, R., Parashare, C., White, S.M., Bastian, T.S.: 2005, Instrument Development for the Green Bank Solar Radio Burst Spectrometer (GB/SRBS). In: Kassim, N., Perez, M., Junor, W., Henning, P. (eds.) *From Clark Lake to the Long Wavelength Array: Bill Erickson's Radio Science*, *Astron. Soc. Pac.* **CS-345**, 357.
- Brown, D.S., Nightingale, R.W., Alexander, D., Schrijver, C.J., Metcalf, T.R., Shine, R.A., Title, A.M., Wolfson, C.J.: 2003, Observations of rotating sunspots from TRACE. *Solar Phys.* **216**, 79–108. doi:10.1023/A:1026138413791.
- Canfield, R.C., Hudson, H.S., McKenzie, D.E.: 1999, Sigmoidal morphology and eruptive solar activity. *Geophys. Res. Lett.* **26**, 627–630. doi:10.1029/1999GL900105.
- Chae, J.: 2007, Measurements of magnetic helicity injected through the solar photosphere. *Adv. Space Res.* **39**, 1700–1705. doi:10.1016/j.asr.2007.01.035.
- Chae, J., Sakurai, T.: 2008, A test of three optical flow techniques-LCT, DAVE, and NAVE. *Astrophys. J.* **689**, 593–612. doi:10.1086/592761.
- Chae, J., Moon, Y.J., Rust, D.M., Wang, H., Goode, P.R.: 2003, Magnetic helicity pumping by twisted flux tube expansion. *Journal of Korean Astronomical Society* **36**, 33–41.
- Chandra, R., Schmieder, B., Mandrini, C.H., Démoulin, P., Pariat, E., Török, T., Uddin, W.: 2011, Homologous flares and magnetic field topology in active region NOAA 10501 on 20 November 2003. *Solar Phys.* **269**, 83–104. doi:10.1007/s11207-010-9670-9.
- Chen, P.F.: 2011, Coronal Mass Ejections: Models and their observational basis. *Living Reviews in Solar Physics* **8**, 1.
- Chen, P.F., Shibata, K.: 2000, An emerging flux trigger mechanism for Coronal Mass Ejections. *Astrophys. J.* **545**, 524–531. doi:10.1086/317803.
- Cho, K.S., Lee, J., Bong, S.C., Kim, Y.H., Joshi, B., Park, Y.D.: 2009, A coronal mass ejection and hard X-ray emissions associated with the kink instability. *Astrophys. J.* **703**, 1–7. doi:10.1088/0004-637X/703/1/1.
- Dabrowski, B.P., Benz, A.O.: 2009, Correlation between decimetric radio emission and hard X-rays in solar flares. *Astron. Astrophys.* **504**, 565–573. doi:10.1051/0004-6361/200811108.
- Démoulin, P., Pariat, E.: 2009, Modelling and observations of photospheric magnetic helicity. *Advances in Space Research* **43**, 1013–1031. doi:10.1016/j.asr.2008.12.004.
- Démoulin, P., Mandrini, C.H., Van Driel-Gesztelyi, L., Lopez Fuentes, M.C., Aulanier, G.: 2002, The Magnetic Helicity Injected by Shearing Motions. *Solar Phys.* **207**, 87–110.
- Fan, Y.: 2009, The Emergence of a twisted flux tube into the solar atmosphere: Sunspot rotations and the formation of a coronal flux rope. *Astrophys. J.* **697**, 1529–1542. doi:10.1088/0004-637X/697/2/1529.
- Foullon, C., Verwichte, E., Nakariakov, V.M., Nykyri, K., Farrugia, C.J.: 2011, Magnetic Kelvin-Helmholtz instability at the Sun. *Astrophys. J. Lett.* **729**, L8. doi:10.1088/2041-8205/729/1/L8.
- Gibson, S.E., Fan, Y., Mandrini, C., Fisher, G., Demoulin, P.: 2004, Observational consequences of a magnetic flux rope emerging into the corona. *Astrophys. J.* **617**, 600–613. doi:10.1086/425294.
- Jiang, Y., Zheng, R., Yang, J., Hong, J., Yi, B., Yang, D.: 2012, Rapid sunspot rotation associated with the X2.2 flare on 2011 February 15. *Astrophys. J.* **744**, 50. doi:10.1088/0004-637X/744/1/50.
- Jockers, K.: 1978, Transport of twist in force-free magnetic flux tubes. *Astrophys. J.* **220**, 1133–1136. doi:10.1086/155998.
- Karlický, M.: 2003, High-frequency radio signatures of solar eruptive flares. *Space Sci. Rev.* **107**, 81–88. doi:10.1023/A:102555218525.

- Karlický, M., Bárta, M.: 2007, Drifting pulsating structures generated during tearing and coalescence processes in a flare current sheet. *Astron. Astrophys.* **464**, 735–740. doi:10.1051/0004-6361:20065983.
- Kliem, B., Karlický, M., Benz, A.O.: 2000, Solar flare radio pulsations as a signature of dynamic magnetic reconnection. *Astron. Astrophys.* **360**, 715–728.
- Kumar, P., Manoharan, P.K., Uddin, W.: 2010a, Evolution of solar magnetic field and associated multiwavelength phenomena: Flare events on 2003 November 20. *Astrophys. J.* **710**, 1195–1204. doi:10.1088/0004-637X/710/2/1195.
- Kumar, P., Srivastava, A.K., Somov, B.V., Manoharan, P.K., Erdélyi, R., Uddin, W.: 2010b, Evidence of solar flare triggering due to loop-loop interaction caused by footpoint shear motion. *Astrophys. J.* **723**, 1651–1664. doi:10.1088/0004-637X/723/2/1651.
- Kumar, P., Srivastava, A.K., Filippov, B., Uddin, W.: 2010c, Multiwavelength study of the M8.9/3B solar flare from AR NOAA 10960. *Solar Phys.* **266**, 39–58. doi:10.1007/s11207-010-9586-4.
- Kumar, P., Srivastava, A.K., Filippov, B., Erdélyi, R., Uddin, W.: 2011, Multiwavelength observations of a failed flux rope in the eruption and associated M-class flare from NOAA AR 11045. *Solar Phys.* **272**, 301–317. doi:10.1007/s11207-011-9829-z.
- Kumar, P., Cho, K.S., Bong, S.C., Park, S.H., Kim, Y.H.: 2012a, Initiation of Coronal Mass Ejection and associated flare caused by helical kink instability observed by SDO/AIA. *Astrophys. J.* **746**, 67. doi:10.1088/0004-637X/746/1/67.
- Kumar, P., Cho, K.S., Chen, P.F., Bong, S.C., Park, S.H.: 2012b, Multiwavelength study of a solar eruption from AR NOAA 1112: II. Large scale coronal wave and loop oscillation. *Solar Phys.*
- Kurokawa, H.: 1987, Two distinct morphological types of magnetic shear development and their relation to flares. *Solar Phys.* **113**, 259–263. doi:10.1007/BF00147706.
- Kusano, K., Yokoyama, T., Maeshiro, T., Sakurai, T.: 2003, Annihilation of magnetic helicity: A new model for solar flare onset. *Advances in Space Research* **32**, 1931–1936. doi:10.1016/S0273-1177(03)90628-4.
- LaBonte, B.J., Georgoulis, M.K., Rust, D.M.: 2007, Survey of magnetic helicity injection in regions producing X-class flares. *Astrophys. J.* **671**, 955–963. doi:10.1086/522682.
- Lemen, J.R., Title, A.M., Akin, D.J., Boerner, P.F., Chou, C., Drake, J.F., Duncan, D.W., Edwards, C.G., Friedlaender, F.M., Heyman, G.F., Hurlburt, N.E., Katz, N.L., Kushner, G.D., Levay, M., Lindgren, R.W., Mathur, D.P., McFeaters, E.L., Mitchell, S., Rehse, R.A., Schrijver, C.J., Springer, L.A., Stern, R.A., Tarbell, T.D., Wuelser, J.P., Wolfson, C.J., Yanari, C., Bookbinder, J.A., Cheimets, P.N., Caldwell, D., Deluca, E.E., Gates, R., Golub, L., Park, S., Podgorski, W.A., Bush, R.I., Scherrer, P.H., Gumm, M.A., Smith, P., Auken, G., Jerram, P., Pool, P., Soufli, R., Windt, D.L., Beardsley, S., Clapp, M., Lang, J., Waltham, N.: 2012, The Atmospheric Imaging Assembly (AIA) on the Solar Dynamics Observatory (SDO). *Solar Phys.* **275**, 17–40. doi:10.1007/s11207-011-9776-8.
- Lin, R.P., Dennis, B.R., Hurford, G.J., Smith, D.M., Zehnder, A., Harvey, P.R., Curtis, D.W., Pankow, D., Turin, P., Bester, M., Csillaghy, A., Lewis, M., Madden, N., van Beek, H.F., Appleby, M., Raudorf, T., McTiernan, J., Ramaty, R., Schmahl, E., Schwartz, R., Krucker, S., Abiad, R., Quinn, T., Berg, P., Hashii, M., Sterling, R., Jackson, R., Pratt, R., Campbell, R.D., Malone, D., Landis, D., Barrington-Leigh, C.P., Slassi-Sennou, S., Cork, C., Clark, D., Amato, D., Orwig, L., Boyle, R., Banks, I.S., Shirey, K., Tolbert, A.K., Zarro, D., Snow, F., Thomsen, K., Henneck, R., McHedlishvili, A., Ming, P., Fivian, M., Jordan, J., Wanner, R., Crubb, J., Preble, J., Matranga, M., Benz, A., Hudson, H., Canfield, R.C., Holman, G.D., Crannell, C., Kosugi, T., Emslie, A.G., Vilmer, N., Brown, J.C., Johns-Krull, C., Aschwanden, M., Metcalf, T., Conway, A.: 2002, The Reuven Ramaty High-Energy Solar Spectroscopic Imager (RHESSI). *Solar Phys.* **210**, 3–32. doi:10.1023/A:1022428818870.
- Longcope, D.W., Welsch, B.T.: 2000, A model for the emergence of a twisted magnetic flux tube. *Astrophys. J.* **545**, 1089–1100. doi:10.1086/317846.
- Luoni, M.L., Démoulin, P., Mandrini, C.H., van Driel-Gesztelyi, L.: 2011, Twisted Flux Tube Emergence Evidenced in Longitudinal Magnetograms: Magnetic Tongues. *Solar Phys.* **270**, 45–74. doi:10.1007/s11207-011-9731-8.
- Magara, T.: 2006, Dynamic and topological features of photospheric and coronal activities produced by flux emergence in the Sun. *Astrophys. J.* **653**, 1499–1509. doi:10.1086/508926.
- Maričić, D., Vršnak, B., Stanger, A.L., Veronig, A.M., Temmer, M., Roša, D.: 2007, Acceleration phase of Coronal Mass Ejections: II. Synchronization of the energy release in the associated flare. *Solar Phys.* **241**, 99–112. doi:10.1007/s11207-007-0291-x.

- Min, S., Chae, J.: 2009, The rotating sunspot in AR 10930. *Solar Phys.* **258**, 203–217. doi:10.1007/s11207-009-9425-7.
- Neupert, W.M.: 1968, Comparison of solar X-Ray line emission with microwave emission during flares. *Astrophys. J. Lett.* **153**, 59–64. doi:10.1086/180220.
- Newkirk, G., Altschuler, M.D.: 1970, Magnetic fields and the solar corona. III: The observed connection between magnetic fields and the density structure of the corona. *Solar Phys.* **13**, 131–152. doi:10.1007/BF00963948.
- Ohya, M., Shibata, K.: 1998, X-Ray plasma ejection associated with an impulsive flare on 1992 October 5: Physical conditions of X-ray plasma ejection. *Astrophys. J.* **499**, 934–944. doi:10.1086/305652.
- Pariat, E., Démoulin, P., Berger, M.A.: 2005, Photospheric flux density of magnetic helicity. *Astron. Astrophys.* **439**, 1191–1203. doi:10.1051/0004-6361:20052663.
- Pariat, E., Démoulin, P., Nindos, A.: 2007, How to improve the maps of magnetic helicity injection in active regions? *Adv. Space Res.* **39**, 1706–1714. doi:10.1016/j.asr.2007.02.047.
- Park, S.H., Chae, J., Wang, H.: 2010, Productivity of solar flares and magnetic helicity injection in active regions. *Astrophys. J.* **718**, 43–51. doi:10.1088/0004-637X/718/1/43.
- Park, S.H., Lee, J., Choe, G.S., Chae, J., Jeong, H., Yang, G., Jing, J., Wang, H.: 2008, The variation of relative magnetic helicity around major flares. *Astrophys. J.* **686**, 1397–1403. doi:10.1086/591117.
- Pesnell, W.D., Thompson, B.J., Chamberlin, P.C.: 2012, The Solar Dynamics Observatory (SDO). *Solar Phys.* **275**, 3–15. doi:10.1007/s11207-011-9841-3.
- Pevtsov, A.A.: 2002, Active-region filaments and X-ray sigmoids. *Solar Phys.* **207**, 111–123. doi:10.1023/A:1015589802234.
- Pevtsov, A.A.: 2008, What helicity can tell us about solar magnetic fields. *Journal of Astrophysics and Astronomy* **29**, 49–56. doi:10.1007/s12036-008-0006-1.
- Pevtsov, A.A., Canfield, R.C., Metcalf, T.R.: 1995, Latitudinal variation of helicity of photospheric magnetic fields. *Astrophys. J. Lett.* **440**, 109–112. doi:10.1086/187773.
- Priest, E.R., Forbes, T.G.: 2002, The magnetic nature of solar flares. *Astron. Astrophys. Rev.* **10**, 313–377. doi:10.1007/s001590100013.
- Régnier, S., Canfield, R.C.: 2006, Evolution of magnetic fields and energetics of flares in active region 8210. *Astron. Astrophys.* **451**, 319–330. doi:10.1051/0004-6361:20054171.
- Rust, D.M., Kumar, A.: 1996, Evidence for helically kinked magnetic flux ropes in solar eruptions. *Astrophys. J. Lett.* **464**, 199–202. doi:10.1086/310118.
- Sakai, J., Nakajima, H., Zaidman, E., Tajima, T., Kosugi, T., Brunel, F.: 1986, Signatures of current loop coalescence in solar flares. In: B. R. Dennis, L. E. Orwig, & A. L. Kiplinger (ed.) *NASA Conference Publication, NASA Conference Publication* **2449**, 393–434.
- Scherrer, P.H., Schou, J., Bush, R.I., Kosovichev, A.G., Bogart, R.S., Hoeksema, J.T., Liu, Y., Duvall, T.L., Zhao, J., Title, A.M., Schrijver, C.J., Tarbell, T.D., Tomczyk, S.: 2012, The Helioseismic and Magnetic Imager (HMI) Investigation for the Solar Dynamics Observatory (SDO). *Solar Phys.* **275**, 207–227. doi:10.1007/s11207-011-9834-2.
- Schou, J., Scherrer, P.H., Bush, R.I., Wachter, R., Couvidat, S., Rabello-Soares, M.C., Bogart, R.S., Hoeksema, J.T., Liu, Y., Duvall, T.L., Akin, D.J., Allard, B.A., Miles, J.W., Rairden, R., Shine, R.A., Tarbell, T.D., Title, A.M., Wolfson, C.J., Elmore, D.F., Norton, A.A., Tomczyk, S.: 2012, Design and Ground Calibration of the Helioseismic and Magnetic Imager (HMI) Instrument on the Solar Dynamics Observatory (SDO). *Solar Phys.* **275**, 229–259. doi:10.1007/s11207-011-9842-2.
- Schuck, P.W.: 2005, Local correlation tracking and the magnetic induction equation. *Astrophys. J. Lett.* **632**, 53–56. doi:10.1086/497633.
- Schuck, P.W.: 2006, Tracking magnetic footpoints with the magnetic induction equation. *Astrophys. J.* **646**, 1358–1391. doi:10.1086/505015.
- Shibata, K., Masuda, S., Shimojo, M., Hara, H., Yokoyama, T., Tsuneta, S., Kosugi, T., Ogawara, Y.: 1995, Hot-plasma ejections associated with compact-loop solar flares. *Astrophys. J. Lett.* **451**, 83–85. doi:10.1086/309688.
- Srivastava, A.K., Zaqarashvili, T.V., Kumar, P., Khodachenko, M.L.: 2010, Observation of kink instability during small B5.0 solar flare on 2007 June 4. *Astrophys. J.* **715**, 292–299. doi:10.1088/0004-637X/715/1/292.
- Stenflo, J.O.: 1969, A Mechanism for the build-up of flare energy. *Solar Phys.* **8**, 115–118. doi:10.1007/BF00150662.
- Su, J., Liu, Y., Liu, J., Mao, X., Zhang, H., Li, H., Wang, X., Xie, W.: 2008, Lorentz force: A possible driving force for sunspot rotation. *Solar Phys.* **252**, 55–71. doi:10.1007/s11207-008-9236-2.

- Temmer, M., Veronig, A.M., Vršnak, B., Rybák, J., Gömöry, P., Stoiser, S., Maričić, D.: 2008, Acceleration in fast halo CMEs and synchronized flare HXR bursts. *Astrophys. J. Lett.* **673**, 95–98. doi:10.1086/527414.
- Temmer, M., Veronig, A.M., Kontar, E.P., Krucker, S., Vršnak, B.: 2010, Combined STEREO/RHESSI study of Coronal Mass Ejection acceleration and particle acceleration in solar flares. *Astrophys. J.* **712**, 1410–1420. doi:10.1088/0004-637X/712/2/1410.
- Tian, L., Alexander, D.: 2006, Role of sunspot and sunspot-group rotation in driving sigmoidal active region eruptions. *Solar Phys.* **233**, 29–43. doi:10.1007/s11207-006-2505-z.
- Tian, L., Alexander, D., Nightingale, R.: 2008, Origins of coronal energy and helicity in NOAA 10030. *Astrophys. J.* **684**, 747–756. doi:10.1086/589492.
- Tokman, M., Bellan, P.M.: 2002, Three-dimensional model of the structure and evolution of Coronal Mass Ejections. *Astrophys. J.* **567**, 1202–1210. doi:10.1086/338699.
- Török, T., Kliem, B.: 2003, The evolution of twisting coronal magnetic flux tubes. *Astron. Astrophys.* **406**, 1043–1059. doi:10.1051/0004-6361:20030692.
- Török, T., Kliem, B.: 2005, Confined and ejective eruptions of kink-unstable flux ropes. *Astrophys. J. Lett.* **630**, 97–100. doi:10.1086/462412.
- Török, T., Chandra, R., Pariat, E., Démoulin, P., Schmieder, B., Aulanier, G., Linton, M.G., Mandrini, C.H.: 2011, Filament interaction modeled by flux rope reconnection. *Astrophys. J.* **728**, 65. doi:10.1088/0004-637X/728/1/65.
- Ueno, S., Nagata, S., Kitai, R., Kurokawa, H.: 2004, Features of solar telescopes at the Hida observatory and the possibilities of coordinated observations with Solar-B. In: T. Sakurai & T. Sekii (ed.) *The Solar-B Mission and the Forefront of Solar Physics*, *Astron. Soc. Pac.* **CS-325**, 319.
- Veronig, A., Vršnak, B., Dennis, B.R., Temmer, M., Hanslmeier, A., Magdalenic, J.: 2002, Investigation of the Neupert effect in solar flares. I. Statistical properties and the evaporation model. *Astron. Astrophys.* **392**, 699–712. doi:10.1051/0004-6361:20020947.
- Yan, X.L., Qu, Z.Q.: 2007, Rapid rotation of a sunspot associated with flares. *Astron. Astrophys.* **468**, 1083–1088. doi:10.1051/0004-6361:20077064.
- Yan, X.L., Qu, Z.Q., Kong, D.F.: 2008, Relationship between rotating sunspots and flare productivity. *Mon. Not. Roy. Astron. Soc.* **391**, 1887–1892. doi:10.1111/j.1365-2966.2008.14002.x.
- Yan, X.L., Qu, Z.Q., Xu, C.L., Xue, Z.K., Kong, D.F.: 2009, The causality between the rapid rotation of a sunspot and an X3.4 flare. *Res. Astron. Astrophys.* **9**, 596–602. doi:10.1088/1674-4527/9/5/010.
- Yokoyama, T., Shibata, K.: 2001, Magnetohydrodynamic simulation of a solar flare with chromospheric evaporation effect based on the magnetic reconnection model. *Astrophys. J.* **549**, 1160–1174. doi:10.1086/319440.
- Zhang, J., Li, L., Song, Q.: 2007, Interaction between a fast rotating sunspot and ephemeral regions as the origin of the major solar event on 2006 December 13. *Astrophys. J. Lett.* **662**, 35–38. doi:10.1086/519280.
- Zhang, Y., Liu, J., Zhang, H.: 2008, Relationship between rotating sunspots and flares. *Solar Phys.* **247**, 39–52. doi:10.1007/s11207-007-9089-0.

